

HD-THEP-00-32
 hep-ph/0007357
 July 2000

Exact and Truncated Dynamics in Nonequilibrium Field Theory

Gert Aarts,* Gian Franco Bonini,‡ and Christof Wetterich||

*Institut für theoretische Physik, Universität Heidelberg
 Philosophenweg 16, 69120 Heidelberg, Germany*

July 31, 2000

Abstract

Nonperturbative dynamics of quantum fields out of equilibrium is often described by the time evolution of a hierarchy of correlation functions, using approximation methods such as Hartree, large N_f , and n PI-effective action techniques. These truncation schemes can be implemented equally well in a classical statistical system, where results can be tested by comparison with the complete nonlinear evolution obtained by numerical methods. For a $1+1$ dimensional scalar field we find that the early-time behaviour is reproduced qualitatively by the Hartree dynamics. The inclusion of direct scattering improves this to the quantitative level. We show that the emergence of nonthermal temperature profiles at intermediate times can be understood in terms of the fixed points of the evolution equations in the Hartree approximation. The form of the profile depends explicitly on the initial ensemble. While the truncated evolution equations do not seem to be able to get away from the fixed point, the full nonlinear evolution shows thermalization with a (surprisingly) slow relaxation.

*email: aarts@thphys.uni-heidelberg.de

‡email: bonini@thphys.uni-heidelberg.de

||email: C.Wetterich@thphys.uni-heidelberg.de

1 Introduction

An understanding of the dynamical evolution of nonequilibrium quantum fields is needed in diverse physical situations as nonrelativistic condensed matter, relativistic heavy-ion colliders, and the early universe. For several reasons a theoretical description is expected to be difficult. First, effective irreversibility has to arise from time-reversal invariant equations. Second, for (asymptotically) late times one expects a nonequilibrium system to thermalize, which implies an effective independence of the initial state, and prescribes a definite value for all correlation functions. Furthermore, during the nonequilibrium evolution, the answer to the question: what dominates the full dynamics at a certain stage, might itself be time-dependent. When approximation methods are used, the chosen method will often need to be modified or replaced as time goes on, to incorporate this shift in importance.

To illuminate this, consider as a prototype for a nonequilibrium system the universe at the end of inflation (see e.g. [1, 2]). In this case several distinct regimes are easily identified. While the early stage is dominated by the oscillating inflaton field, in the intermediate regime the created quanta scatter both with the inflaton and with each other, leading to a partial energy redistribution between the modes. Finally, in the last stage subsequent interactions are expected to bring the universe to thermal equilibrium. It is a great theoretical challenge to describe these various stages in a unified way.

Although in principle the time evolution of expectation values is determined completely, after the initial density matrix is given, by the microscopic Heisenberg equations of motion, this is in practice only of minor help, due to the absence of exact solutions or solution methods. Consider for example a simple scalar quantum field theory with a quartic interaction. The Heisenberg equation of motion determines the time evolution of the mean field,

$$(\partial_t^2 - \nabla_x^2 + m^2)\langle\phi(x, t)\rangle = -\lambda\langle\phi^3(x, t)\rangle/2, \quad (1)$$

where the brackets indicate the expectation value with respect to the initial density matrix. This equation requires knowledge of the three-point function $\langle\phi^3(x, t)\rangle$. The equation for the three-point function itself involves the five-point function (in general $n + 2$ -point functions are needed to solve the exact evolution for n -point functions), which leads to a full hierarchy of coupled equations. In most cases a solution to this hierarchy is not available, and it becomes of interest to find approximation schemes that capture the essential part of the full dynamics as correctly as possible.

A widely-used approach is to truncate the infinite hierarchy of correlation functions. One of the simplest truncations is the Hartree approximation in which at most two-point functions appear, and the three-point function is replaced by $\langle\phi^3(x, t)\rangle = 3\langle\phi(x, t)\rangle\langle\phi^2(x, t)\rangle$. A systematic way to implement this is by using a large N_f expansion, where N_f denotes the number of e.g. scalar or fermion fields

[3] (for applications, see e.g. [4, 5, 6, 7]). The main drawback of these Gaussian truncations is that in homogeneous or translationally invariant ensembles scattering is absent, which limits the range of validity. This feature has been an important stimulation to improve upon the homogeneous Hartree and large N_f approximations. One possibility is to allow for inhomogeneous mean fields. In that case scattering via the space-dependent mean field $\langle\phi(x, t)\rangle$ is present in the effective equations (see e.g. [8] for analytical investigations and [9] for a numerical study). Another natural extension is to go beyond the Gaussian approximation and include higher nontrivial correlation functions [10, 11, 12], guided e.g. by the large N_f expansion to next-to-leading order. This typically results in effective equations that are nonlocal in time. From a practical (numerical) point of view, it is desirable to use effective equations that are local in time, as in the Hartree approximation. This has motivated the use of the 1PI-effective action for equal-time correlation functions [13, 14, 15]. Truncated at quartic order this includes scattering and all $1/N_f$ corrections [16]. A discussion of the structure of dynamical equations for equal-time correlation functions in the large N_f expansion up to and including $1/N_f^2$ terms can be found in [17]. Finally, very promising results have been obtained recently [18], using a truncation of the 2PI-effective action at next-to-leading order. The resulting equations are nonlocal in time, i.e. they require the integration of memory kernels. For a $1 + 1$ dimensional field theory this appears, however, not to be a numerical obstacle.

In all cases, it would be desirable to perform a direct test of these methods and their range of validity. Unfortunately a comparison with the full nonperturbative evolution in the quantum field theory cannot be made, due to the absence of exact methods. In the case of quantum mechanics on the other hand, such tests can be performed, and the evolution from a Hartree factorization, a $1/N_f$ expansion at leading and next-to-leading order, and other extensions beyond the Gaussian approximation have been compared with the exact evolution obtained by numerically solving the Schrödinger equation [10, 11]. It is, however, not obvious how the lessons learned from quantum mechanics with one degree of freedom can be translated to field theory with (in principle infinitely) many degrees of freedom. Both scattering and the possibility of taking the thermodynamic limit are absent in the quantum mechanical case.

The situation in classical field theory is completely different. Here the full evolution can be simulated using Monte Carlo methods and numerical integration: initial conditions are generated by sampling according to the initial probability distribution, and the subsequent time evolution follows from solving the classical equations of motion, which can be done numerically. Expectation values are then constructed by summing over many independent realizations. When the number of initial conditions is taken larger and larger, the initial probability distribution is approximated better and better, and the resulting time evolution will become exact, in principle. As we will see below, it is possible to implement many of the approximation methods discussed above for the quantum field theoretical case

also in a classical field theory. The reason is that the methods do not directly touch upon the quantum nature, but instead state how to truncate a hierarchy of correlation functions, which is present in a classical statistical system as well. Therefore, we focus in this paper on nonequilibrium evolution in classical field theory, formulated on a spatial lattice to regularize the theory. Note that the role of the thermodynamic limit may be investigated keeping the lattice spacing fixed. The general strategy is to compare the truncated dynamics with the numerical results obtained from sampling initial conditions from a given initial probability distribution. Our hope is that the insights obtained below will survive when going to the quantum field theory.

In the remainder of the Introduction we give the outline of the paper. As a simple toy model we consider a classical scalar field theory in $1 + 1$ dimensions, with the (continuum) action

$$S = \int dt dx \left[\frac{1}{2}(\partial_t \phi)^2 - \frac{1}{2}(\partial_x \phi)^2 - \frac{1}{2}m^2 \phi^2 - \frac{\lambda}{8}\phi^4 \right]. \quad (2)$$

In the next section we show how the (homogeneous) Hartree approximation can be implemented in the classical theory. In Sec. 3 we discuss evolution equations obtained from a functional differential equation for the equal-time 1PI effective action. A truncation of the time-dependent effective action at quadratic order gives evolution equations that are equivalent to those obtained in the Hartree approximation. Scattering is incorporated by a truncation of the effective action that includes momentum-dependent four-point functions. In Sec. 4 the choice of initial probability distribution and some numerical and lattice aspects are discussed. We have divided the comparison between the truncated evolution equations and the lattice results in two parts. In Sec. 5 we discuss the early and intermediate times, where the system is still relatively far from thermal equilibrium. The late-time regime, where thermal equilibrium is approached, is described in Sec. 6. Our findings are summarized in Sec. 7.

2 Classical Hartree approximation

The classical problem is fully specified by the equation of motion

$$\partial_t^2 \phi(x, t) = [\partial_x^2 - m^2] \phi(x, t) - \lambda \phi^3(x, t)/2, \quad (3)$$

supplemented with initial conditions for $\phi(x, t)$ and $\pi(x, t) = \partial_t \phi(x, t)$. These initial conditions are determined by the initial probability distribution $\rho[\pi(x), \phi(x)]$, where $\phi(x) = \phi(x, 0)$, $\pi(x) = \pi(x, 0)$. The choice of initial distribution is not needed at this stage, we only assume that the ensemble is translationally invariant in space and respects the discrete symmetry $\phi \rightarrow -\phi$, $\pi \rightarrow -\pi$. The average with respect to the initial distribution will be denoted with brackets $\langle \cdot \rangle$. Our aim

is to find evolution equations for (equal-time) correlation functions of the field $\phi(x, t)$ and the canonical momentum $\pi(x, t)$.

As discussed in the Introduction, a widely-used approach in quantum field theory is the Hartree approximation. This can be implemented in the classical theory as well, and a brute but simple way to do this is as follows. If we assume a Hartree-type factorization for the interaction term in the classical equation, i.e., $\lambda\phi^3 \rightarrow 3\lambda\phi\langle\phi^2\rangle$, we find

$$\partial_t^2\phi(x, t) = \left[\partial_x^2 - m^2 - \frac{3}{2}\lambda\langle\phi^2(x, t)\rangle\right]\phi(x, t). \quad (4)$$

In the case of translationally invariant ensembles, $\langle\phi^2(x, t)\rangle$ is independent of x and the equation can be written in momentum space as

$$\partial_t^2\phi(q, t) = -\bar{\omega}_q^2\phi(q, t), \quad (5)$$

with the effective frequency squared

$$\bar{\omega}_q^2 = \omega_q^2 + \frac{3}{2}\lambda\langle\phi^2\rangle, \quad (6)$$

where $\omega_q^2 = q^2 + m^2$, and $\langle\phi^2\rangle = \langle\phi^2(x, t)\rangle$. In the case of N_f scalar fields with a complete $O(N_f)$ symmetry, the second term on the right-hand-side of Eq. (6) is multiplied by $(N_f + 2)/(3N_f)$. In this paper we restrict ourselves to the case $N_f = 1$. Note, however, that there is no problem in principle to extend the analysis below to finite $N_f > 1$. The unequal-time two-point function

$$S(x - y; t, t') = \langle\phi(x, t)\phi(y, t')\rangle = \int \frac{dq}{2\pi} e^{iq(x-y)} S(q; t, t'), \quad (7)$$

obeys in this approximation the usual mean-field equation of motion

$$\left[\partial_t^2 + \bar{\omega}_q^2\right] S(q; t, t') = 0, \quad (8)$$

where the effective frequency is determined from the two-point function at equal time:

$$\bar{\omega}_q^2 = \omega_q^2 + \frac{3}{2}\lambda \int \frac{dp}{2\pi} S(p; t, t). \quad (9)$$

Note that modes with a given momentum q only interact with the homogeneous mean-field background, so that direct scattering between different momentum modes is absent.

The dynamics can be written equivalently¹ in terms of equal-time expectation values, at the expense of introducing more than one two-point function. The

¹In the sense that the evolution equations presented below are obtained from the same starting point (5).

following four combinations are a priori independent:

$$\begin{aligned} G_{\phi\phi}(x-y, t) &= \langle \phi(x, t)\phi(y, t) \rangle, \\ G_{\pi\pi}(x-y, t) &= \langle \pi(x, t)\pi(y, t) \rangle, \\ G_{\pi\phi}(x-y, t) &= \frac{1}{2}\langle \pi(x, t)\phi(y, t) + \phi(x, t)\pi(y, t) \rangle, \end{aligned} \quad (10)$$

and the parity-odd combination

$$G_{\pi\phi}^{\text{odd}}(x-y, t) = \langle \pi(x, t)\phi(y, t) - \phi(x, t)\pi(y, t) \rangle. \quad (11)$$

The dynamical equations are conveniently written in momentum space, according to

$$G_{\phi\phi}(q, t) = \int dx e^{-iqx} G_{\phi\phi}(x, t), \quad (12)$$

etc., and they couple only the combinations (10):

$$\begin{aligned} \partial_t G_{\phi\phi}(q, t) &= 2G_{\pi\phi}(q, t), \\ \partial_t G_{\pi\phi}(q, t) &= -\bar{\omega}_q^2 G_{\phi\phi}(q, t) + G_{\pi\pi}(q, t), \\ \partial_t G_{\pi\pi}(q, t) &= -2\bar{\omega}_q^2 G_{\pi\phi}(q, t). \end{aligned} \quad (13)$$

The fourth combination $G_{\pi\phi}^{\text{odd}}(q)$ is exactly conserved under the Hartree equations and does not enter in the dynamics. It is zero in the case that the ensemble is invariant under space reflection.

In the Hartree approximation a nontrivial combination of two-point functions, termed α^2 in [14], is conserved,

$$\alpha^{-2}(q) = G_{\phi\phi}(q, t)G_{\pi\pi}(q, t) - G_{\pi\phi}^2(q, t), \quad (14)$$

for each q . This can be understood from the absence of scattering or mode mixing at this order and the resulting symmetry (see Appendix A). Finally, the Hartree equations conserve the expectation value of the energy,

$$E_{\text{Hartree}} = L \int \frac{dq}{2\pi} \left[\frac{1}{2}G_{\pi\pi}(q, t) + \frac{1}{2} \left(\omega_q^2 + \frac{3\lambda}{4} \int \frac{dp}{2\pi} G_{\phi\phi}(p, t) \right) G_{\phi\phi}(q, t) \right], \quad (15)$$

which can be obtained using a Gaussian factorization of the ϕ^4 -term in the microscopic expression for the energy, or from the effective Lagrangian given in Appendix A.

3 Equal-time effective action

In order to improve upon the Hartree approximation, it is necessary to include direct scattering contributions in the evolution equations. We aim here at a

formulation that is local in time. This is also desirable from a numerical point of view.² One way to achieve this is by employing a formalism based on the equal-time effective action $\Gamma[\phi, \pi; t]$, the generating functional of 1PI equal-time correlation functions [13]. The effective action obeys the following (functional) evolution equation [14, 16]

$$\partial_t \Gamma[\phi, \pi; t] = -\mathcal{L}_{\text{cl}} \Gamma[\phi, \pi; t], \quad (16)$$

with

$$\begin{aligned} \mathcal{L}_{\text{cl}} = & \int dx \left[\pi(x) \frac{\delta}{\delta \phi(x)} + \phi(x) \left(\partial_x^2 - m^2 - \frac{1}{2} \lambda \left[\phi^2(x) + 3\bar{G}_{\phi\phi}(x, x) \right] \right) \frac{\delta}{\delta \pi(x)} \right. \\ & - \int dx_1 dx_2 dx_3 \bar{G}_{\phi\psi_1}(x, x_1) \bar{G}_{\phi\psi_2}(x, x_2) \bar{G}_{\phi\psi_3}(x, x_3) \\ & \left. \times \frac{\delta^3 \Gamma}{\delta \psi_1(x_1) \delta \psi_2(x_2) \delta \psi_3(x_3)} \frac{\delta}{\delta \pi(x)} \right]. \end{aligned} \quad (17)$$

Here $\psi \equiv (\phi, \pi)$ and $\bar{G}_{\psi\psi'}(x, x')$ denotes the full (matrix) propagator in arbitrary field background, obtained from Γ as

$$\bar{G}_{\psi\psi'}^{-1}(x, y) = \frac{\delta^2 \Gamma}{\delta \psi(x) \psi'(y)}. \quad (18)$$

The full propagator evaluated at zero background is written without the bar. The effective action depends on ‘effective’ fields ϕ and π , which are defined via the Legendre transformation, relating Γ and $\ln Z$ in the usual way [13]. Though we use the same notation, these fields should not be confused with the microscopic fields that appear in the original action (2).

In order to solve the exact evolution equation (16), some approximation has to be made. This brings us back to the issue of truncations, as discussed in the previous sections. We use a truncation or ansatz that includes all 1PI n -point functions, with $n \leq 4$, and respects the symmetry $\psi \rightarrow -\psi$ as well as spatial translation and reflection. The ansatz reads

$$\begin{aligned} \Gamma[\phi, \pi; t] = & \int_q \left[\frac{1}{2} A(q) \phi^*(q) \phi(q) + \frac{1}{2} B(q) \pi^*(q) \pi(q) + C(q) \pi^*(q) \phi(q) \right] \\ & + \frac{1}{8} \int_{q_1, q_2, q_3, q_4} 2\pi \delta(q_1 + q_2 + q_3 + q_4) \left[u(q_1, q_2, q_3) \phi(q_1) \phi(q_2) \phi(q_3) \phi(q_4) \right. \\ & + v(q_1, q_2, q_3) \pi(q_1) \phi(q_2) \phi(q_3) \phi(q_4) + w(q_1, q_2, q_3) \pi(q_1) \pi(q_2) \phi(q_3) \phi(q_4) \\ & \left. + y(q_1, q_2, q_3) \pi(q_1) \pi(q_2) \pi(q_3) \phi(q_4) + z(q_1, q_2, q_3) \pi(q_1) \pi(q_2) \pi(q_3) \pi(q_4) \right]. \end{aligned}$$

We use the shorthand

$$\int_q = \int \frac{dq}{2\pi},$$

²See however [18] for a successful implementation of time-nonlocal evolution equations.

and suppress the time dependence of the two-point couplings A, B, C , the four-point couplings u, v, w, y, z , and the correlation functions $G_{\psi\psi'}$ in this section.

The matrix relation (18) at vanishing background can now be given explicitly, and

$$\begin{aligned} G_{\phi\phi}(q) &= B(q)/\alpha^2, \\ G_{\pi\phi}(q) &= -C(q)/\alpha^2, \\ G_{\pi\pi}(q) &= A(q)/\alpha^2, \end{aligned} \quad (19)$$

with the determinant

$$\alpha^2(q) = A(q)B(q) - C^2(q). \quad (20)$$

This definition of $\alpha(q)$ is equivalent to that in Eq. (14). For future convenience we introduce

$$c(q) \equiv \frac{C(q)}{B(q)}, \quad (21)$$

which will be used to convert two-point functions:

$$G_{\pi\phi}(q) = -c(q)G_{\phi\phi}(q). \quad (22)$$

The time dependence of the effective action determined by (16) translates into evolution equations for the couplings. Exact flow equations for the two-point functions follow from taking the second derivatives of Eq. (16) with respect to ϕ and π at $\phi = \pi = 0$:³

$$\begin{aligned} \partial_t A(q) &= 2\tilde{\omega}_q^2 C(q) \\ \partial_t B(q) &= -2C(q) - 2\gamma(q)B(q) \\ \partial_t C(q) &= -A(q) + \tilde{\omega}_q^2 B(q) - \gamma(q)C(q), \end{aligned} \quad (23)$$

with the frequency squared

$$\begin{aligned} \tilde{\omega}_q^2 &= \omega_q^2 + \frac{3\lambda}{2} \int_p G_{\phi\phi}(p) \\ &\quad - \frac{3\lambda}{8} \int_{q_1, q_2, q_3} 2\pi\delta(q - q_1 - q_2 - q_3) G_{\phi\phi}(q_1)G_{\phi\phi}(q_2)G_{\phi\phi}(q_3) \left[4u(q_1, q_2, q_3) \right. \\ &\quad \left. - 3c(q_1)v(q_1, q_2, q_3) + 2c(q_1)c(q_2)w(q_1, q_2, q_3) - c(q_1)c(q_2)c(q_3)y(q_1, q_2, q_3) \right], \end{aligned} \quad (24)$$

where we recognize the free part, the Hartree term, and a contribution with the topology of the setting-sun diagram, containing three full propagators and a

³The equations presented below are slightly simpler than the ones that can be obtained from setting $N_f = 1$ in the equations for the $O(N_f)$ model [16].

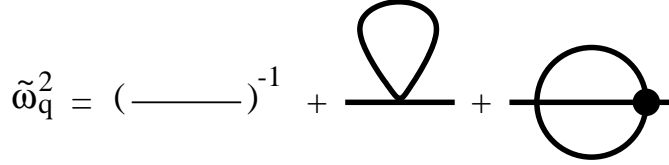


Figure 1: Graphical representation of the effective frequency squared, Eq. (24). The thick (thin) lines denote the full (free) equal-time two-point function $G_{\phi\phi}$. The blob in the setting-sun diagram is a full equal-time vertex function.

(complicated) dynamical vertex function (see Fig. 1). The other factor appearing in (23) has a setting-sun structure as well:

$$\begin{aligned} \gamma(q) = & \frac{3\lambda}{8} \int_{q_1, q_2, q_3} 2\pi\delta(q - q_1 - q_2 - q_3) G_{\phi\phi}(q_1) G_{\phi\phi}(q_2) G_{\phi\phi}(q_3) [v(q, -q_1, -q_2) \\ & - 2c(q_1)w(-q_1, q, -q_2) + c(q_2)c(q_3)\{y(q_3, q_2, -q) + 2y(-q, q_1, q_3)\} \\ & - 4c(q_1)c(q_2)c(q_3)z(-q_1, q, -q_2)]. \end{aligned} \quad (25)$$

These equations have to be completed with the evolution equations for the four-point couplings, and those are listed in Appendix B. Note that $\alpha(q)$ is no longer a conserved quantity as it is in the Hartree approximation, but obeys $\partial_t\alpha(q) = -\gamma(q)\alpha(q)$.

Finally, the evolution equations conserve exactly the energy

$$\begin{aligned} E_\Gamma = & E_{\text{Hartree}} - \frac{3}{8}\lambda \int_{q_1, q_2, q_3, q_4} 2\pi\delta(q_1 + q_2 + q_3 + q_4) G_{\phi\phi}(q_1) G_{\phi\phi}(q_2) \\ & \times G_{\phi\phi}(q_3) G_{\phi\phi}(q_4) [u(q_1, q_2, q_3) - c(q_1)v(q_1, q_2, q_3) + c(q_1)c(q_2)w(q_1, q_2, q_3) \\ & - c(q_1)c(q_2)c(q_3)y(q_1, q_2, q_3) + c(q_1)c(q_2)c(q_3)c(q_4)z(q_1, q_2, q_3)]. \end{aligned} \quad (26)$$

It is illuminating to make a connection with the Hartree equations derived in the preceding section. A truncation of the effective action at quadratic order gives dynamical equations involving only A , B , and C . It is straightforward to check that these give precisely the Hartree equations (13) for the equal-time two-point functions.

The equal-time effective action permits an easy inclusion of quantum effects [19]. The Hartree approximation does not distinguish between classical and quantum field theories. In the quartic truncation the quantum effects add simple terms to the evolution equations of the quartic couplings [14]. A direct verification of the truncated evolution for quantum fields is obviously much harder.

4 Initial ensemble and lattice discretization

For an investigation of the time evolution of correlation functions we need to specify the initial ensemble or probability distribution. In this paper we choose

to start from a Gaussian, translationally invariant ensemble. The reasons to take an initially Gaussian ensemble are the following: first of all, the Hartree equations truncate the dynamics to Gaussian dynamics for all times. Therefore, possible truncation effects will show up during the time evolution only, but not already initially, since the initial ensemble is treated correctly in the Hartree approximation. Furthermore, Gaussian ensembles are the ones that are often considered in *quantum* field theory away from equilibrium. It is straightforward to construct an initial density matrix that leads to Gaussian correlation functions, and vice versa. Finally, from a technical point of view, Gaussian ensembles can easily be implemented in both the truncated evolution equations and the numerical evolution obtained by sampling initial conditions.

In the set of Gaussian ensembles, we choose to take the equilibrium distribution function of the unperturbed Hamiltonian H_0 , where

$$\begin{aligned} H &= \int dx \left[\frac{1}{2}\pi^2 + \frac{1}{2}(\partial_x\phi)^2 + \frac{1}{2}m^2\phi^2 + \frac{\lambda}{8}\phi^4 \right] \\ &= H_0 + V, \quad V = \int dx \frac{\lambda}{8}\phi^4. \end{aligned} \quad (27)$$

Thus, the initial probability distribution is given by

$$\rho[\pi(x), \phi(x)] = Z_0^{-1} \exp[-H_0/T_0], \quad Z_0 = \int \mathcal{D}\pi \mathcal{D}\phi \exp[-H_0/T_0], \quad (28)$$

where $\phi(x) = \phi(x, 0)$, $\pi(x) = \pi(x, 0)$, and

$$\int \mathcal{D}\pi \mathcal{D}\phi = \int \prod_x d\pi(x) d\phi(x) \quad (29)$$

denotes the integral over the initial phase-space. The temperature of the initial ensemble is denoted with T_0 . Note that this distribution function is of course not the equilibrium distribution for nonzero λ .

Since the ensemble is Gaussian, the only nontrivial correlation functions at $t = 0$ are the two-point functions, and they read

$$\begin{aligned} \langle \phi(q)\phi(q') \rangle &= G_{\phi\phi}(q, 0)2\pi\delta(q + q'), & G_{\phi\phi}(q, 0) &= T_0/(q^2 + m^2), \\ \langle \pi(q)\pi(q') \rangle &= G_{\pi\pi}(q, 0)2\pi\delta(q + q'), & G_{\pi\pi}(q, 0) &= T_0. \end{aligned} \quad (30)$$

Possible variations of this initial ensemble would be to choose different ‘initial temperatures’ $T_0(q)$ for each momentum mode and the ϕ and π fields.

To properly define the model, we formulate it on a lattice in space with spacing a . The number of spatial sites is N , such that the volume is $L = Na$, and we use periodic boundary conditions. Due to the finite volume and lattice cutoff, the momentum q takes a finite number of discrete values:

$$q = \frac{2\pi k}{L}, \quad k = \left\{ -\frac{N}{2} + 1, \dots, \frac{N}{2} \right\}, \quad (31)$$

and momentum integrals are replaced by sums: $\int dq/(2\pi) \rightarrow L^{-1} \sum_q$. The dispersion relation is modified due to the Laplacian on the lattice and reads

$$\omega_q^2 = \hat{q}^2 + m^2, \quad \hat{q}^2 = \frac{2}{a^2}(1 - \cos aq). \quad (32)$$

Classical field theory suffers from the Rayleigh-Jeans divergence, which implies that the lattice cutoff cannot be taken to zero in a straightforward manner. Indeed, the expectation value of the full energy in this ensemble is

$$\langle H \rangle = \langle H_0 \rangle + \langle V \rangle = L \left[\frac{T_0}{a} + \frac{3\lambda}{8} \langle \phi^2 \rangle^2 \right] = N \left[T_0 + a \frac{3\lambda}{8} \langle \phi^2 \rangle^2 \right], \quad (33)$$

where the first explicit expression is written such that the extensivity of the energy and the linear divergence as $a \rightarrow 0$ are manifest, and the second one on the other hand emphasizes ‘classical equipartition’ in a system with N degrees of freedom. In this paper we work at fixed lattice cutoff $ma = 0.25$ (corresponding to a fixed momentum cutoff $\Lambda = \pi/a = 4\pi m$). The thermodynamic limit can be taken by increasing the number of lattice sites N , keeping the initial temperature T_0 fixed.

The expectation value $\langle \phi^2 \rangle$ can be calculated at $t = 0$:

$$\langle \phi^2(x) \rangle = \frac{1}{L} \sum_q G_{\phi\phi}(q, 0) = \frac{1}{L} \sum_q \frac{T_0}{\hat{q}^2 + m^2} \equiv \frac{T_0}{m} I. \quad (34)$$

The sum is ultraviolet finite. For the lattice sizes we use its value is close to the infinite volume value: $I = \frac{1}{2}[1 + a^2 m^2 / 4]^{-1/2} \simeq 0.5$.

The initial conditions for the evolution equations can now be given explicitly. They read

$$\begin{aligned} A(q, 0) &= G_{\phi\phi}^{-1}(q, 0) = (\hat{q}^2 + m^2)/T_0, \\ B(q, 0) &= G_{\pi\pi}^{-1}(q, 0) = 1/T_0, \end{aligned} \quad (35)$$

and

$$\begin{aligned} C(q, 0) &= u(q_1, q_2, q_3; 0) = v(q_1, q_2, q_3; 0) \\ &= w(q_1, q_2, q_3; 0) = y(q_1, q_2, q_3; 0) = z(q_1, q_2, q_3; 0) = 0. \end{aligned} \quad (36)$$

The evolution equations are solved using a standard fourth-order Runge-Kutta algorithm that is exactly time reversible.

The full nonlinear evolution is constructed by sampling initial conditions from the Gaussian ensemble (30) and solving the equation of motion numerically for each initial condition in real space. In order to do this, the action is discretized on a lattice in time as well, with step size $a_0 < a$. The resulting discretized equations of motion are of the leap-frog type. We have used $a_0/a = 0.05$ and

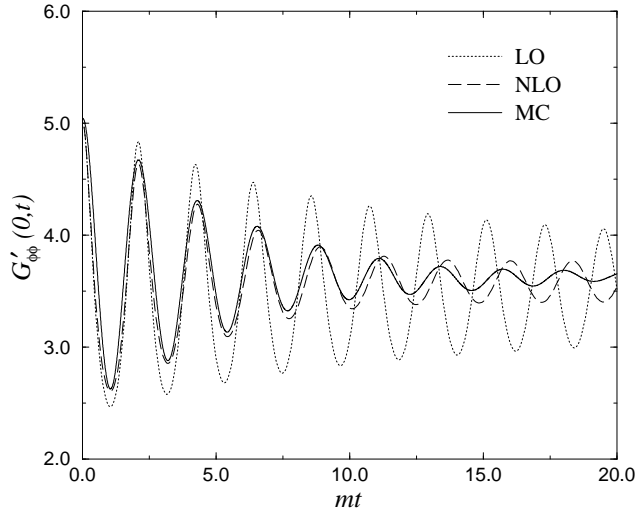


Figure 2: Time evolution of the two-point function $G'_{\phi\phi}(0, t)$. We compare the Hartree equations (LO, $N = 512$), the next-to-leading order equations (NLO, $N = 160$), and the results from a Monte Carlo sampling ($N = 512, N_m = 16,000$). In Figs. 2-8 the initial temperature of the Gaussian ensemble is $T'_0 = 5$. In all figures, the lattice spacing is $ma = 0.25$.

0.01, and checked independence of the step size. The ensemble is approximated by using many independent initial conditions. The number of ensemble members is denoted with N_m . For the results presented below we have used $N_m \sim 2,500 - 16,000$.

Finally, for the numerical analysis it is convenient to use the mass parameter m as the dimensionful scale. Therefore we rescale all dimensionful parameters with the appropriate power of m . Rescaled variables will be denoted with a prime. Furthermore, the classical equation of motion (3) can be made independent of the coupling λ by introducing a field ϕ' as

$$\phi' = \sqrt{3\lambda/m^2} \phi. \quad (37)$$

The rescaled (dimensionless) canonical momentum is $\pi' = (3\lambda/m^4)^{1/2}\pi$ and the dimensionless energy reads $E' = 3\lambda E/m^3$. We define a dimensionless temperature $T' = 3\lambda T/m^3$ such that $E/T = E'/T'$. As a result, besides the lattice parameters $a' = ma$ and N ($L' = a'N$), only one parameter remains to be specified:

$$T'_0 \equiv \frac{3\lambda}{m^3} T_0. \quad (38)$$

A larger value of T'_0 corresponds to a larger effective interaction strength.⁴

⁴A quick way to change to primed variables is to put $m = 1, \lambda = 1/3$.

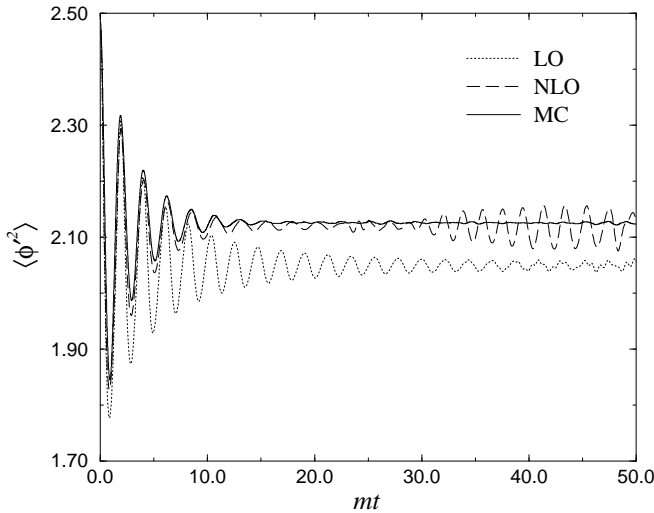


Figure 3: Time evolution of $\langle \phi'^2(x, t) \rangle = L'^{-1} \sum_q G'_{\phi\phi}(q, t)$. The initial value is $\langle \phi'^2 \rangle = T'_0 I = 2.5$. The time-averaged values in the interval $20 < mt < 50$ are 2.049 (LO), 2.114 (NLO), and 2.126(5) (MC). The Hartree fixed-point value (see below) is 2.056.

5 Early and intermediate times

We are now fully equipped to compare the time evolution using the different methods. For shortness, we refer below to the evolution obtained in the Hartree approximation as LO (leading order) and the evolution from the equal-time effective action truncated up to four-point couplings as NLO (next-to-leading order). Although in principle there is no small parameter governing the truncation, we use the labeling common in the large N_f expansion, since the Hartree approximation is closely related to the leading-order contribution in $1/N_f$. The full nonlinear evolution of a sample of initial conditions is denoted with MC (Monte Carlo).

The equal-time two-point function at zero momentum $G_{\phi\phi}(q = 0, t)$ is shown in Fig. 2, for a typical choice of parameters. The numerical integration of the NLO evolution is rather time consuming, due to the presence of the four-point couplings u, v, w, y , and z that depend on three independent momentum variables. Therefore it is not possible to take as large volumes as in LO and MC. However, we have checked that at this stage this does not affect the comparison. It is clear that the first few oscillations are well approximated by both LO and NLO dynamics. We will refer to this period as the early-time regime. It is visible that the Hartree evolution underestimates damping whereas the size of the oscillations in NLO remains comparable with the MC result much longer. Around $mt = 10$ the periods of oscillation in NLO and MC evolution start to disagree.

The crucial quantity in the mean-field approximation (4) is the field squared

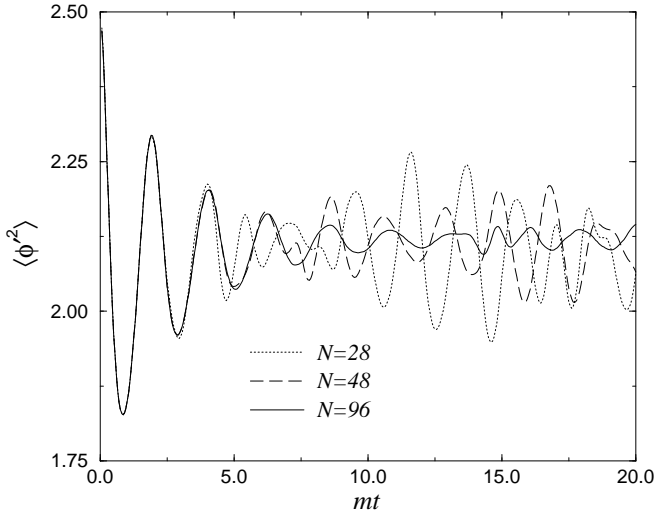


Figure 4: Volume dependence: NLO evolution of $\langle\phi'^2\rangle$. In a smaller volume the evolution deviates earlier from the large-volume limit. Damping can be seen only in the period before the evolution starts to deviate.

$\langle\phi^2(x, t)\rangle = L^{-1} \sum_q G_{\phi\phi}(q, t)$ which is presented in Fig. 3. Again we see that the first few oscillations are in good agreement. Then a difference becomes visible between LO on the one hand, and NLO and MC on the other hand: at LO the amplitude of oscillations reduces slower (less damping) and the averaged value lies below the other two. A comparison of the time-averaged values between $20 < mt < 50$ shows that the Hartree result differs by a few percent from NLO and MC. The time-averaged value in NLO is surprisingly close to the MC result.

After the initial reduction the size of fluctuations increases again in NLO around $mt = 30$. To investigate this issue, we study the volume dependence of the evolution in NLO. The phenomenon of ‘resurgence of fluctuations’ is presented in Fig. 4 for relatively small volumes. We see that fluctuations become large again after the initial reduction and that the evolution becomes undamped. The time when this occurs increases with the volume. We stress that this effect is not physical, as it is absent in the MC result, nor is it generated by errors in the numerical integration. Rather, it is a property of the NLO approximation. Since this seems to be an important limitation for the validity of NLO, we analyse the thermodynamic limit and the consistency of the NLO evolution on a quantitative level. We compare the dynamics for different volume sizes with the largest one that is available ($N = 160$). For an equal-time observable $O(t)$, we define the difference

$$\Delta O_N(t) = \frac{|\langle O_N(t) \rangle - \langle O_{160}(t) \rangle|}{\langle O_{160} \rangle_{\text{av}}}. \quad (39)$$

The normalization $\langle O_{160}(t) \rangle_{\text{av}}$ is the time-averaged value of $\langle O_{160}(t) \rangle$ between $0 < mt < 20$, and is used to set the scale. We denote the time where $\Delta O_N(t)$

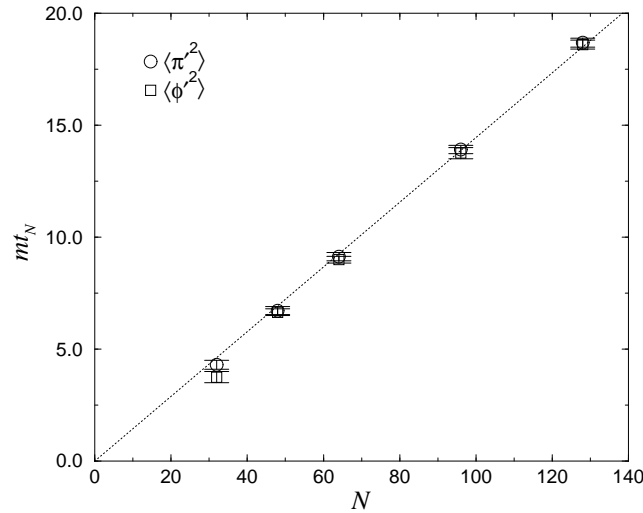


Figure 5: Thermodynamic limit in the NLO evolution: volume dependence of the time mt_N where $\Delta O_N(t)$ exceeds 0.005 (see text), for $O = \pi'^2(x, t)$ and $\phi'^2(x, t)$. The dashed line is a straight-line fit through the origin.

exceeds the conservative bound of 0.005 by t_N . The dependence of t_N on the volume is shown in Fig. 5. It turns out that t_N is sensitive to the details of the evolution, due to the oscillating character of $\Delta O_N(t)$. This sensitivity is indicated with error bars. We see that in a larger volume the evolution behaves better for a longer time, and that this time increases roughly linearly with the system size. We emphasize that the possibility of taking the thermodynamic limit distinguishes the comparison performed in this paper with those where quantum mechanics was used to test the truncated evolution. For this aspect classical fields are closer to quantum fields than quantum mechanics is.

At a later moment, to which we will refer as t_u , fluctuations grow rapidly and the numerical evolution becomes uncontrolled. Typically t_u is much larger than t_N . We have checked that the time where the evolution starts to behave badly is not an artefact of the numerical integration. For instance, reducing the step size by a factor of 5 does not affect the results. A similar behaviour has been noted before in a system of anharmonic oscillators in $0 + 1$ dimensions [15]. The breakdown of the evolution equations beyond leading order at large times has also been observed for quantum mechanics [11].

Fixed points in the Hartree approximation

From the viewpoint of thermalization, the most interesting observable is $G_{\pi\pi}(q, t)$. In an interacting theory the equilibrium value is $G_{\pi\pi}^{\text{eq}}(q) = T$ for all q . Away from equilibrium we define therefore an ‘effective temperature’ for a momentum mode

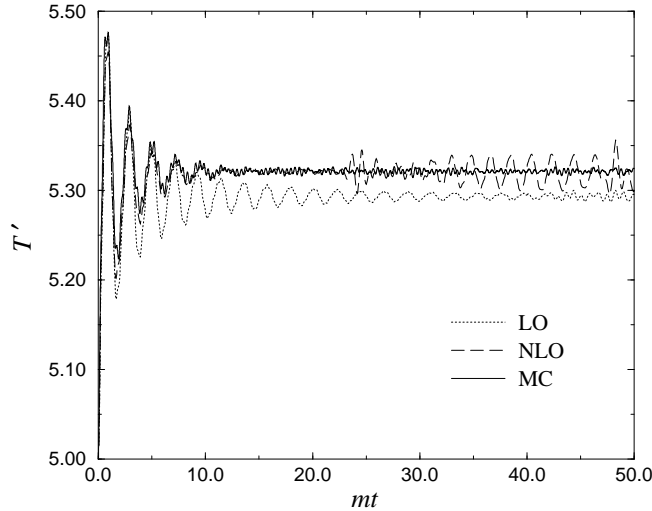


Figure 6: Time evolution of the effective temperature $T'(t) = N^{-1} \sum_q G'_{\pi\pi}(q, t)$. The time-averaged values in the interval $20 < mt < 50$ are 5.293 (LO), 5.318 (NLO), and 5.321(4) (MC). The value at the Hartree fixed point is 5.291.

q :

$$T(q, t) \equiv G_{\pi\pi}(q, t), \quad (40)$$

and the average temperature over all modes

$$T(t) = N^{-1} \sum_q G_{\pi\pi}(q, t) = a\langle\pi^2\rangle. \quad (41)$$

Because of our choice of initial ensemble all momentum modes have initially the same (noninteracting) temperature T_0 , so that $G_{\pi\pi}(q, 0)$ is flat in momentum space. Due to the nonzero coupling it deviates from being flat immediately after $t = 0$. For later times deviation from ‘flatness’ of $G_{\pi\pi}(q, t)$ is a good measure for deviation from thermal equilibrium.

In Fig. 6 we show the average temperature T' as a function of time. The qualitative aspects comparing LO, NLO, and MC are the same as in Fig. 3. Furthermore we see many rapid oscillations with a small amplitude which were absent in Fig. 3. The reason is that $\langle\phi^2\rangle$ is ultraviolet finite and therefore dominated by the low-momentum modes, while $\langle\pi^2\rangle$ is sensitive to all frequencies up to the lattice cutoff.

Fig. 6 gives the impression that the system establishes a new temperature $T' \approx 5.32 \neq T'_0 = 5$ rather quickly. However, in order to be in thermal equilibrium, all momentum modes should have the same temperature. In Fig. 7 the effective temperature $T'(q, t)$ for three momentum modes is shown. Perhaps surprisingly, we see that for each q $T'(q, t)$ oscillates around a different value. The mean values appear rather stable and do not seem to approach each other. This resembles the nonthermal fixed points discussed in [16] for the NLO equations.

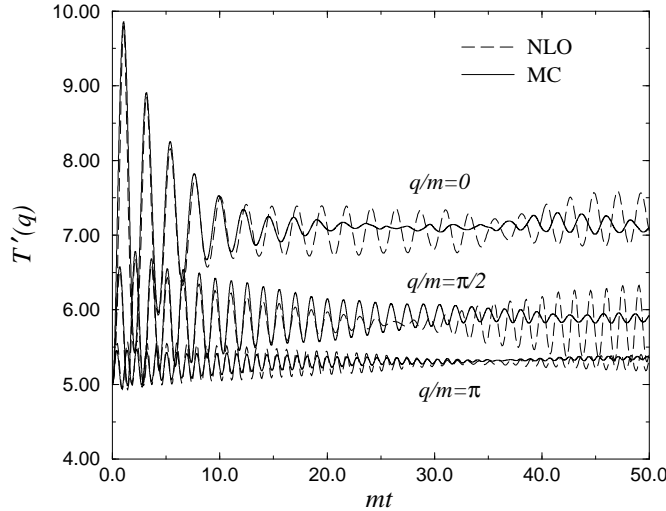


Figure 7: Time evolution of the mode-temperature $T'(q, t) = G'_{\pi\pi}(q, t)$ for modes $q/m = 0, \pi/2, \pi$. The initial value is $T'_0 = 5$ for all q . The LO result is not shown for clarity.

In fact, it turns out that this behaviour can be understood with satisfactory accuracy already in terms of fixed or stationary points of the evolution equations in the Hartree approximation. The relations between the two-point functions at a fixed point (denoted with a star) are readily determined from the Hartree equations (13), and read

$$G_{\pi\pi}^*(q) = \bar{\omega}_q^{*2} G_{\phi\phi}^*(q), \quad G_{\pi\phi}^*(q) = 0, \quad (42)$$

with

$$\bar{\omega}_q^{*2} = \omega_q^2 + \frac{3}{2} \lambda \langle \phi^2 \rangle^*. \quad (43)$$

The first equation shows an expected relation between $\pi\pi$ and $\phi\phi$ two-point functions, the second expression confirms that the time-reflection odd two-point function has to vanish at a stationary point.

The fixed-point structure of the Hartree equations by itself does not yet constrain the allowed fixed-point solutions completely. However, we can supplement the set of equations (42) with the nontrivial combinations $\alpha^2(q)$, given in Eq. (14), that are exactly conserved for each momentum mode q independently. At a fixed point this gives a third relation

$$G_{\pi\pi}^*(q) G_{\phi\phi}^*(q) = \alpha^{-2}(q). \quad (44)$$

We recall that $\alpha(q)$ can be determined from the initial ensemble. Combining (42) and (44) yields the complete fixed-point solution

$$G_{\pi\pi}^*(q) = \frac{\bar{\omega}_q^*}{\alpha(q)}, \quad (45)$$

$$G_{\phi\phi}^*(q) = \frac{1}{\bar{\omega}_q^* \alpha(q)}. \quad (46)$$

Since $G_{\pi\pi}^*(q)$ is identified with the effective temperature for a mode q , the first equation shows that at a fixed point the system will generically be nonthermal, since the temperature of a mode depends on its momentum, and that the nonthermal ‘temperature profile’ follows directly from the initial ensemble. The second expression leads to a gap equation, after an integration over q ,

$$\langle \phi^2 \rangle^* \equiv \int \frac{dq}{2\pi} G_{\phi\phi}^*(q) = \int \frac{dq}{2\pi} \frac{1}{\bar{\omega}_q^* \alpha(q)}, \quad (47)$$

since the right-hand side depends on $\langle \phi^2 \rangle^*$ via $\bar{\omega}_q^*$. We would like to stress again that for an arbitrary initial ensemble the fixed point in the Hartree approximation is determined completely and all its properties can be calculated.

We will now become explicit and specialize to the Gaussian initial ensemble we consider in this paper. From the initial expectation values (30) one finds

$$\alpha(q) = \frac{\omega_q}{T_0}, \quad (48)$$

so that the gap equation reads

$$\langle \phi^2 \rangle^* = T_0 \int \frac{dq}{2\pi} \frac{1}{\bar{\omega}_q^* \omega_q}. \quad (49)$$

It is convenient to introduce the dimensionless parameter $\Delta = 3\lambda\langle \phi^2 \rangle^*/(2m^2) = \langle \phi'^2 \rangle^*/2$, so that the above equation can be written as

$$\Delta = \frac{T'_0}{2\pi} \frac{1}{\sqrt{1+\Delta}} F\left(\frac{\pi}{2}, \sqrt{\frac{\Delta}{1+\Delta}}\right), \quad (50)$$

where $F(\pi/2, k)$ is the (complete) elliptic function of the first kind, and we recall that $T'_0 = 3\lambda T_0/m^3$. This gap equation can be solved numerically. For $T'_0 = 5$, we find $\langle \phi'^2 \rangle^* = 2\Delta = 2.06$, which can be compared with the time-averaged value of the LO, NLO, and MC evolution in Fig. 3.

For the effective momentum-dependent temperature at the fixed point we find

$$T^*(q) = G_{\pi\pi}^*(q) = T_0 \frac{\bar{\omega}_q^*}{\omega_q} = T_0 \left[1 + \frac{3}{2} \frac{\lambda\langle \phi^2 \rangle^*}{\omega_q^2} \right]^{1/2}. \quad (51)$$

In order to compare this profile with the numerical results, we calculate the time average of $T'(q, t)$ between $0 < mt < 50$ for the LO, NLO, and MC evolution. The result is shown in Fig. 8. We see that the temperature profile emerging dynamically in the Hartree approximation is extremely well described by its fixed-point shape (51). The result from MC turns out to be remarkably close, implying

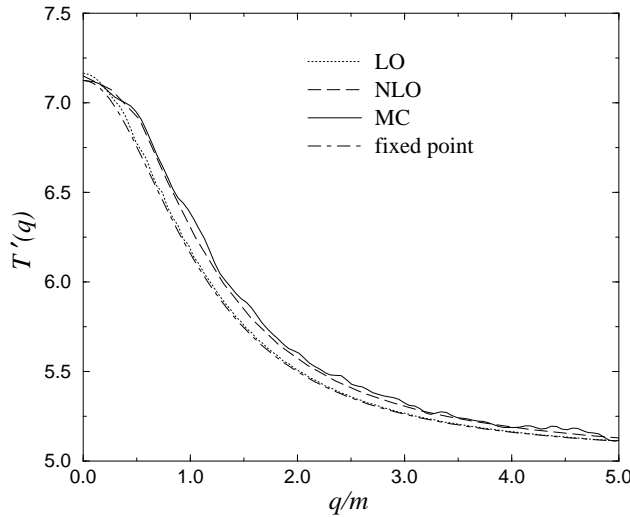


Figure 8: Temperature profile: effective mode-temperature $T'(q)$ versus momentum q/m after time averaging over the interval $0 < mt < 50$, for the LO, NLO, and MC evolution. The fourth line is the analytic expression at the fixed point of the Hartree equations, with $\langle \phi'^2 \rangle^* = 2.06$ from the fixed-point gap equation.

that the full nonlinearity only has a small quantitative effect at this stage, and that direct scattering is not very important. Also, the NLO profile is close to the MC result, showing that the inclusion of momentum-dependent four-point functions in the truncation of the effective action improves the agreement with the full evolution. Finally, the frequency of oscillation of the individual two-point functions $G_{\psi\psi'}$ (or A , B , and C) is approximately $2\bar{\omega}^*$, which can be seen in Fig. 7 for $G_{\pi\pi}(q, t)$. We refer to the stage where the dynamics is well described by the Hartree fixed point as the intermediate-time regime.

At next-to-leading order, the fixed-point structure changes and becomes much more complicated. From time-reflection symmetry, it is clear that the two-point function $C(q, t)$, and the four-point couplings $v(q_1, q_2, q_3; t)$ and $y(q_1, q_2, q_3; t)$ have to vanish at a fixed point. This implies that also $\gamma(q, t)$ vanishes. However, the other four-point couplings cannot be zero at a fixed point, which can be seen e.g. from the dynamical equation for $v(q_1, q_2, q_3; t)$ in Appendix B. Therefore the fixed point is determined by a set of integral equations. Furthermore, the relation of the fixed point to the initial ensemble may be rather complicated.

6 Late times and thermalization

The results in the previous section show that in the intermediate-time regime correlation functions appear quasi-stationary but are not thermal. In particular the time-averaged value of $G_{\pi\pi}(q, t)$ is well described by the nonthermal profile

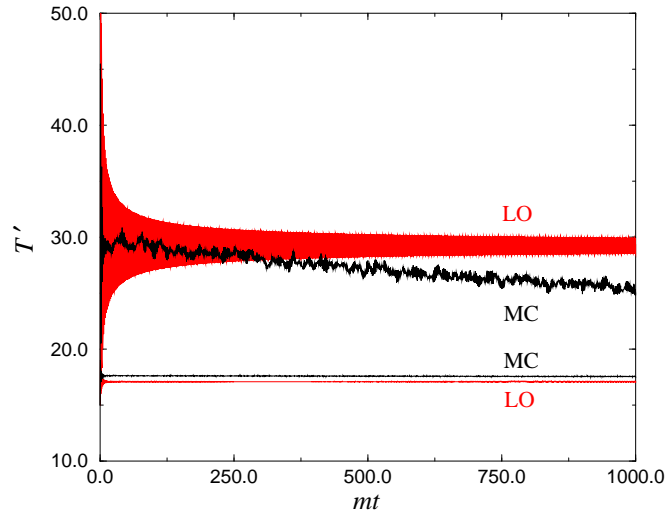


Figure 9: Time evolution of the zero-mode temperature $T'(0, t)$ (two upper lines) from LO ($N = 8192$) and MC ($N = 128, N_m = 12,500$). The Hartree fixed-point value is 28.5. The average temperatures over all modes $T'(t)$ (two lower lines) appear as straight lines with the MC result slightly above the LO result. The initial temperature of the Gaussian ensemble is $T'_0 = 15$.

(51), determined from the fixed point of the Hartree equations. Since the MC profile is, up to a small quantitative correction, in agreement with (51) as well, we infer that this (quasi-)fixed point plays a role also in the full nonlinear evolution.

The fate of the fixed point can be determined by going to longer times. In Fig. 9 we show the evolution of the effective temperature of the zero-momentum mode for LO and MC. We have chosen a higher value for T'_0 than before. Also shown are the average temperature over all modes, $T'(t)$. As was already mentioned in Sec. 5, the equilibrium temperature, which we will denote with T' , is established very early in the evolution, so that the lines presenting $T'(t)$ appear straight. We see that at LO the zero mode remains oscillating around approximately 29.2. We have calculated the fixed-point value for $T'_0 = 15$ and found $T'^*(q = 0) = 28.5$. The full nonlinear evolution, on the other hand, shows a decrease towards T' : the approach to thermal equilibrium. We also see that the damping at LO is unrelated to the MC result. It is clear that whereas the Hartree approximation describes the early and intermediate regimes qualitatively (or even quantitatively), it is not able to move away from the fixed point and the approximation breaks down completely in the late-time regime.

Unfortunately, for accessible volume sizes the NLO evolution cannot reach the relevant time scales before becoming unreliable (see the discussion around Figs. 4, 5). At the largest possible times where the evolution could still be followed, we have not been able to see a sign of thermalization.

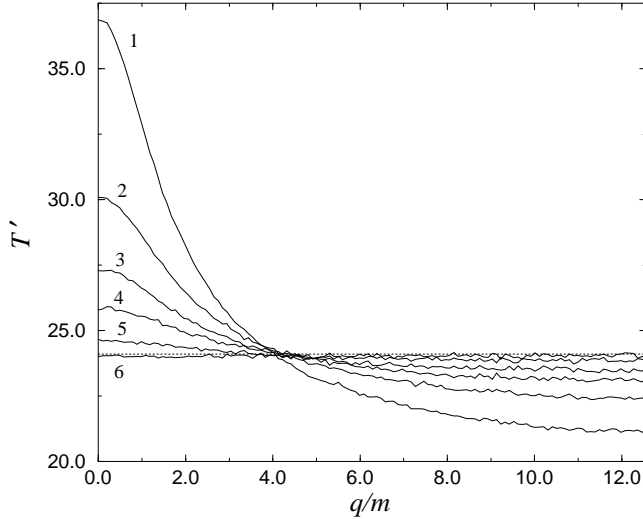


Figure 10: Approach to equilibrium: (time-averaged) snapshots of the momentum-dependent temperature $T'(q, t)$ for all the modes up to cutoff $\Lambda/m = 4\pi$. The curves represent a time average over an interval $(t_i - \Delta t, t_i)$, with $m\Delta t = 1500$, and $mt_1 = 1500$ (1), 3000 (2), 4500 (3), 6000 (4), 9000 (5), and 15000 (6). Line 6 is hardly distinguishable from the dotted horizontal line, which is the average temperature from all modes ($T' = 24.01$). The parameters are $T'_0 = 20$, $N = 256$, $N_m = 2,500$ (in Figs. 10-12 MC only).

We continue with MC only. As indicated above, a good observable to follow during the thermalization stage is the temperature profile $G_{\pi\pi}(q, t)$, which should become flat (q -independent). The evolution from the fixed-point profile at intermediate times to a thermal profile at late times is presented in Fig. 10. We show the time dependence of $T'(q, t)$ for all modes up to the lattice cutoff, averaged over an interval $m\Delta t = 1500$, for six intervals. In the first few intervals, the presence of the nonthermal profile is still visible. As time goes on, the profile becomes flatter and flatter. In the last interval shown, between $mt = 13500$ and 15000, the profile appears q -independent and can hardly be distinguished from the straight line, $T' = 24.01$. We see that all momentum modes obtain the same temperature T' roughly at the same time. For a detailed investigation on the issue of thermalization in this model concerning other correlation functions than $G_{\pi\pi}$ we refer to our previous paper [20]. The aspects of thermalization we studied there are complementary to our findings here (in Ref. [20] we focused on the independence of initial conditions, the long-time behaviour of temporal averages in single ‘microstates’ and other (non-Gaussian) initial ensembles, and the role of the thermodynamic limit).

To determine the time scale for thermalization, we concentrate on the zero mode. In Fig. 11 we show the relaxation of $T'(0, t)$ towards the average temper-

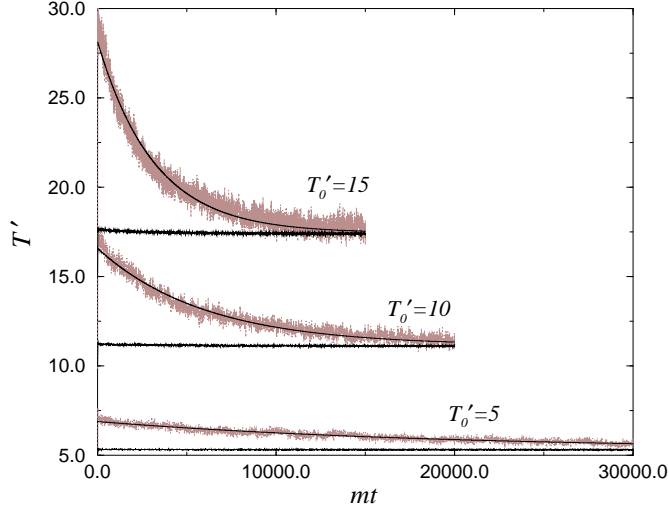


Figure 11: Relaxation of the zero-mode temperature $T'(0, t)$ to the average temperature for three values of the initial temperature T'_0 . The average temperatures $T'(t)$ from all modes appear as straight lines. Also shown are exponential fits, explained in the text. The parameters are $N = 128$, $N_m = 5,000$ each.

ature $T'(t)$ for three different initial temperatures T'_0 . The numerical data are fitted with an exponential of the form

$$T'(0, t) = T' \left[1 + \kappa e^{-t/\tau} \right]. \quad (52)$$

The fit is performed over the whole time interval.⁵ The resulting relaxation rate $1/m\tau$ is shown in Fig. 12 versus the equilibrium temperature T' , for two system sizes, at fixed lattice spacing $ma = 0.25$. No volume dependence is visible.

In the remainder of this section, we discuss the thermalization time scale. In a quantum theory, the relaxation rate is in general related to the imaginary part of the self-energy [21]. A recent analysis, applying the relaxation-time approximation to a weakly coupled quantum scalar field in $3 + 1$ dimensions, can be found in [22]. At weak coupling, the rate is determined by the imaginary part of the setting-sun diagram, describing an on-shell two-to-two scattering process, $\omega_{\mathbf{p}} + \omega_{\mathbf{k}} \rightarrow \omega_{\mathbf{q}} + \omega_{\mathbf{p}-\mathbf{k}-\mathbf{q}}$. In Appendix C we show how to implement a relaxation-rate (linear response) approximation for a classical field close to equilibrium. We also give the calculation of the imaginary part of the classical setting-sun diagram in $1 + 1$ dimensions, taken on-shell for arbitrary external spatial momentum.

One should note, however, that in $1+1$ dimensions on-shell two-to-two scattering is special, since the energy-conservation relation has only two simple solutions: $q = -k$ and $q = p$. Both solutions give $\omega_p + \omega_k \rightarrow \omega_p + \omega_k$, and scattering events of

⁵We also checked for possible power law corrections to the exponential relaxation, but found no indication for those.

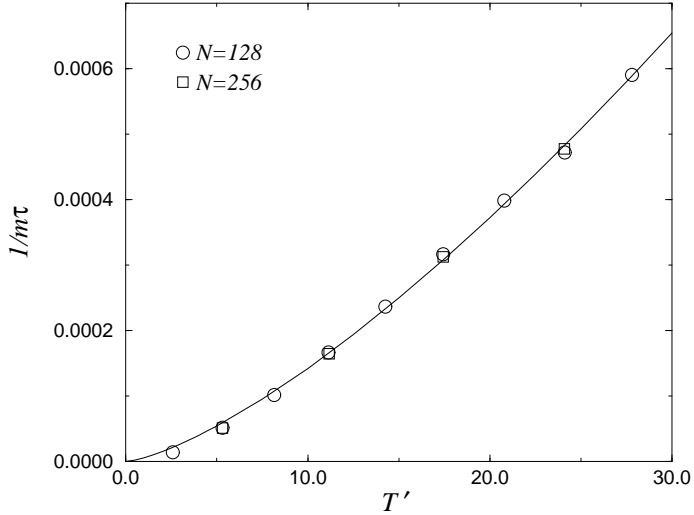


Figure 12: Relaxation rate $1/m\tau$ of the zero-mode $T'(0, t)$ versus the final equilibrium temperature T' . The initial temperatures are $T'_0 = 2.5, 5, 7.5, \dots, 22.5$, for $N = 128$ using $N_m = 5,000$ initial conditions for each temperature, and $T'_0 = 5, 10, 15, 20$ for $N = 256$ ($N_m = 2,500$). Statistical errors are smaller than the symbol sizes. The line is a phenomenological power law fit of the $N = 128$ data, $1/m\tau = 5.8 \cdot 10^{-6} (T')^{1.39}$.

this type do not change the population numbers for the participating momentum modes. We find in Appendix C that the naively computed ‘relaxation rate’ is several orders of magnitude bigger than the thermalization rate observed in the numerical simulations.

Processes with nontrivial momentum exchange are necessary for thermalization. This goes beyond two-to-two scattering and occurs only at higher order. It is possible that a resummation of the self-energy to two-loop order (i.e. including a resummation of the setting-sun diagram) will determine the relevant time scale. This is suggested by the results found in [18], where (quantum) evolution equations for the two-point function are solved. Those equations contain a setting-sun type contribution with fully dressed (in a self-consistent manner) propagators. This would also cure the collinear singularity that appears in the lowest-order setting-sun diagram, both in the quantum and in the classical theory (see Appendix C).

7 Outlook

We have investigated the nonequilibrium time evolution of correlation functions in field theories. In order to gain an understanding of the validity of approximations often used for quantum fields away from equilibrium, we argued that it is

useful to consider the equivalent problem in classical field theory. Taking 1+1 dimensional classical ϕ^4 theory, discretized on a lattice, as a simple (but often used) model, we have implemented a Hartree approximation and a truncation for equal-time correlation functions containing scattering. The truncated dynamics was compared with the fully nonlinear results from a numerical sampling of initial conditions. We believe that our findings are relevant for the 3 + 1 dimensional quantum theory as well.

For the investigated initial Gaussian ensembles the evolution at early and intermediate times is well reproduced by both truncations. We found that the Hartree approximation underestimates damping. This difference becomes more pronounced at larger coupling. The inclusion of scattering leads to a quantitatively better agreement with the full numerical evolution.

There is an intermediate-time regime in which correlation functions have non-thermal values. The characteristic behaviour in this regime can be understood from the presence of a nonthermal quasi-stationary point, which is close to a fixed point in the Hartree approximation. As a consequence of (infinitely many) conserved correlation functions, the Hartree approximation cannot move away from this fixed point and is therefore unable to describe thermalization.

The quartic approximation to the equal-time effective action (NLO) suffers from a different problem. For a finite system (N finite) the initially very successful description of the evolution moves away from both the infinite-volume evolution at NLO and the numerical results at some time t_N . For $t > t_N$ fluctuations grow that are related to the truncation and not to the physical system. We find that t_N is proportional to N , such that the problem may disappear for $N \rightarrow \infty$. In practice this is of little help, since only finite N can be investigated numerically. At a time $t_u \gg t_N$ the evolution becomes uncontrolled and cannot be followed numerically. For accessible values of N , both t_N and t_u are found to be (much) smaller than the typical relaxation time for thermalization. For this reason, we do not know whether NLO is *in principle* able to describe thermalization or not.

Since the late-time regime can certainly not be described by the Hartree approximation, and the quartic approximation including scattering becomes unreliable on the relevant large time scales, we conclude that the regime of thermalization is still unsolved in the approach using evolution equations for equal-time correlation functions.

Concerning the late-time regime, promising results for translationally invariant ensembles have been obtained recently using an unequal-time formulation that is time-nonlocal [18]. It would be interesting to implement the method employed there in a classical theory and carry out a similar comparison as we did in this paper for the equal-time formulations. An open question in that respect is whether a successful truncation can be found in an equal-time formalism as well or if the nonlocality is crucial for an analytical description of the thermalization regime.

Acknowledgements

G.A. would like to thank Jan Smit for useful discussions. This work was supported by the TMR network *Finite Temperature Phase Transitions in Particle Physics*, EU contract no. FMRX-CT97-0122.

A Symmetry at leading order

The Hartree equations conserve the combination $\alpha(q)$, defined in Eq. (14), for each q . This can be understood as follows [4]. The effective equations can be rewritten by introducing a set of complex variables $\xi(q, t)$ as

$$\begin{aligned} G_{\phi\phi}(q, t) &= \xi^*(q, t)\xi(q, t), \\ G_{\pi\phi}(q, t) &= \frac{1}{2} \left[\dot{\xi}^*(q, t)\xi(q, t) + \xi^*(q, t)\dot{\xi}(q, t) \right], \\ G_{\pi\pi}(q, t) &= \dot{\xi}^*(q, t)\dot{\xi}(q, t). \end{aligned} \quad (53)$$

In terms of these the evolution equations (13) read

$$\ddot{\xi}(q, t) = - \left(\omega_q^2 + \frac{3}{2}\lambda \int \frac{dp}{2\pi} |\xi(p, t)|^2 \right) \xi(q, t). \quad (54)$$

This equation can be derived from an effective Lagrange density

$$\mathcal{L}_{\text{eff}} = \int \frac{dq}{2\pi} \left[|\dot{\xi}(q, t)|^2 - \left(\omega_q^2 + \frac{3}{4}\lambda \int \frac{dp}{2\pi} |\xi(p, t)|^2 \right) |\xi(q, t)|^2 \right], \quad (55)$$

which has a global (i.e. time independent) symmetry $\xi(q, t) \rightarrow \exp[i\theta(q)]\xi(q, t)$ for each q . The corresponding conserved charge reads

$$Q(q) = i \left[\xi^*(q, t)\dot{\xi}(q, t) - \dot{\xi}^*(q, t)\xi(q, t) \right]. \quad (56)$$

This charge is in fact the conserved quantity and $Q(q) = 2\alpha^{-1}(q)$.

B Evolution of the four-point couplings

In this Appendix we list the equations that determine the time evolution of the four-point couplings. Again, these equations are slightly simpler than the ones that can be obtained from setting $N_f = 1$ in the equations for the $O(N_f)$ model [16].

The evolution equations read:

$$\begin{aligned} \partial_t u(q_1, q_2, q_3) &= [\tilde{\omega}_{q_1}^2 v(q_1, q_2, q_3) + 4\lambda C(q_1) - 4\lambda C(q_2)S_1(q_1 + q_2, q_3)]_{SYM}, \\ \partial_t v(q_1, q_2, q_3) &= [2\tilde{\omega}_{q_2}^2 w(q_1, q_2, q_3) - 4u(q_1, q_2, q_3) + 4\lambda B(q_1) \end{aligned}$$

$$\begin{aligned}
& -\gamma(q_1)v(q_1, q_2, q_3) - 4\lambda\{B(q_1)S_1(q_1 + q_2, q_3) \\
& + C(q_4)S_3(q_1 + q_2, q_1) + 2C(q_2)S_5(q_2 + q_3, q_1)\}]_{SYM}, \\
\partial_t w(q_1, q_2, q_3) &= [3\tilde{\omega}_{q_3}^2 y(q_1, q_2, q_3) - v(q_1, q_2, q_3) - 2v(q_2, q_4, q_1) \\
& - \{\gamma(q_1) + \gamma(q_2)\}w(q_1, q_2, q_3) - \lambda\{C(q_3)S_4(q_1, q_2) \\
& + 8B(q_2)S_5(q_2 + q_3, q_1)\} - 4\lambda B(q_1)S_3(-q_1 - q_3, q_2)]_{SYM}, \\
\partial_t y(q_1, q_2, q_3) &= [4\tilde{\omega}_{q_4}^2 z(q_1, q_2, q_3) - 2w(q_1, q_2, q_3) \\
& - [\gamma(q_1) + \gamma(q_2) + \gamma(q_3)]y(q_1, q_2, q_3) - \lambda B(q_3)S_4(q_1, q_2)]_{SYM} \\
\partial_t z(q_1, q_2, q_3) &= -[y(q_1, q_2, q_3) + 4\gamma(q_1)z(q_1, q_2, q_3)]_{SYM},
\end{aligned}$$

where the subscript SYM implies symmetrization with respect to the appropriate permutations of q_1 , q_2 , q_3 , and $q_4 = -(q_1 + q_2 + q_3)$. Here we have used the one-loop integrals

$$\begin{aligned}
S_1(q_1, q_2) &= \frac{3}{4} \int_{p_1, p_2} 2\pi\delta(p_2 - p_1 - q_1) G_{\phi\phi}(p_1)G_{\phi\phi}(p_2) [6u(p_2, -p_1, q_2) \\
& - 3c(p_1)v(-p_1, p_2, q_2) + c(p_1)c(p_2)w(-p_1, p_2, q_2)], \\
S_3(q_1, q_2) &= \frac{1}{4} \int_{p_1, p_2} 2\pi\delta(p_2 - p_1 + q_1) G_{\phi\phi}(p_1)G_{\phi\phi}(p_2) [7v(q_2, -p_1, p_2) \\
& - 8c(p_2)w(p_2, q_2, -p_1) + 7c(p_1)c(p_2)y(p_2, -p_1, q_2)], \\
S_4(q_1, q_2) &= 3 \int_{p_1, p_2} 2\pi\delta(p_2 - p_1 + q_1 + q_2) G_{\phi\phi}(p_1)G_{\phi\phi}(p_2) [w(q_1, q_2, p_2) \\
& - 3c(p_1)y(q_1, q_2, -p_1) + 6c(p_1)c(p_2)z(p_2, -p_1, q_1)], \\
S_5(q_1, q_2) &= \frac{1}{4} \int_{p_1, p_2} 2\pi\delta(p_2 + p_1 + q_1) G_{\phi\phi}(p_1)G_{\phi\phi}(p_2) [v(q_2, -p_1, -p_2) \\
& - 2c(p_1)w(-p_1, q_2, -p_2) + c(p_1)c(-p_2)y(q_2, -p_1, -p_2)].
\end{aligned}$$

C Relaxation-time approximation

For a quantum field slightly away from equilibrium the relation between the imaginary part of the self-energy and the thermalization rate for the single-particle distribution function has been pointed out long ago by Weldon [21]. A more recent detailed analysis can be found in [22] for a scalar field in $3 + 1$ dimensions. Here we briefly outline the arguments of [22] in $d + 1$ dimensions and then show how to adapt those for the *classical* theory we consider here. This analysis is valid for a weakly coupled plasma, close to equilibrium.

A dynamical equation for the (quasi-)particle distribution $n(\mathbf{p}, t)$, describing the relaxation towards the Bose distribution $n_B(\omega_{\mathbf{p}}) = 1/[\exp(\omega_{\mathbf{p}}/T) - 1]$, can be obtained perturbatively, using the Heisenberg equations of motion and resumming hard thermal loops if necessary. In the relaxation-time approximation, the distribution function for a momentum mode \mathbf{p} is written as

$$n(\mathbf{p}, t) = n_B(\omega_{\mathbf{p}}) + \delta n(\mathbf{p}, t). \quad (57)$$

All other modes $\mathbf{q} \neq \mathbf{p}$ are assumed to be in equilibrium. Skipping many steps [22], the resulting linearized equation is

$$\partial_t \delta n(\mathbf{p}, t) = -\Gamma(\mathbf{p}) \delta n(\mathbf{p}, t), \quad (58)$$

with the relaxation rate

$$\Gamma(\mathbf{p}) = -\frac{\text{Im } \Sigma(\omega_{\mathbf{p}}, \mathbf{p})}{\omega_{\mathbf{p}}}. \quad (59)$$

This rate is twice the plasmon damping rate $\gamma(\mathbf{p})$. For a weakly coupled scalar field with a ϕ^4 interaction in 3+1 dimensions, $\Gamma(\mathbf{p})$ is determined by the imaginary part of the setting-sun diagram.

For the classical theory our interest is in the evolution of the momentum-dependent ‘temperature’ $T(\mathbf{p}, t) = G_{\pi\pi}(\mathbf{p}, t)$. We may obtain this correlation function from the classical unequal-time two-point function $S(\mathbf{x} - \mathbf{y}; t_1, t_2) = \langle \phi(\mathbf{x}, t_1) \phi(\mathbf{y}, t_2) \rangle$ by a spatial Fourier transform as

$$T(\mathbf{p}, t) = \partial_{t_1} \partial_{t_2} S(\mathbf{p}; t_1, t_2) \Big|_{t_1=t_2=t}. \quad (60)$$

A calculation of $S(\mathbf{p}; t_1, t_2)$ using classical perturbation theory to second order in the coupling constant can be found in [23] for $d = 3$ (see also [24]). The resulting expressions are similar to the quantum ones. The most important change is that the Bose distributions are replaced by classical distribution functions

$$n_{\text{cl}}(\omega_{\mathbf{p}}) = \frac{T}{\omega_{\mathbf{p}}}. \quad (61)$$

The relevant second-order contribution reads [23]

$$\begin{aligned} S_2(\mathbf{p}; t_1, t_2) = & - \int_0^\infty dt' dt'' G_0^R(\mathbf{p}, t_1 - t') \Sigma_{R,\text{cl}}(\mathbf{p}, t' - t'') S_0(\mathbf{p}, t'' - t_2) \\ & - \int_0^\infty dt' dt'' S_0(\mathbf{p}, t_1 - t') \Sigma_{A,\text{cl}}(\mathbf{p}, t' - t'') G_0^A(\mathbf{p}, t'' - t_2) \\ & - \int_0^\infty dt' dt'' G_0^R(\mathbf{p}, t_1 - t') \Sigma_{F,\text{cl}}(\mathbf{p}, t' - t'') G_0^A(\mathbf{p}, t'' - t_2), \end{aligned}$$

where

$$S_0(\mathbf{p}, t) = n_{\text{cl}}(\omega_{\mathbf{p}}) \frac{\cos \omega_{\mathbf{p}} t}{\omega_{\mathbf{p}}} \quad (62)$$

is the free two-point function. The free retarded Green function reads

$$G_0^R(\mathbf{p}, t) = \theta(t) \frac{\sin \omega_{\mathbf{p}} t}{\omega_{\mathbf{p}}} = G_0^A(\mathbf{p}, -t), \quad (63)$$

and the self-energy corrections are, in $d + 1$ dimensions,

$$\begin{aligned} \Sigma_{R,\text{cl}}(\mathbf{p}, t) &= -\frac{9\lambda^2}{2} \int_{\mathbf{k}, \mathbf{q}} S_0(\mathbf{k}, t) S_0(\mathbf{q}, t) G_0^R(\mathbf{p} - \mathbf{k} - \mathbf{q}, t) = \Sigma_{A,\text{cl}}(\mathbf{p}, -t), \\ \Sigma_{F,\text{cl}}(\mathbf{p}, t) &= -\frac{9\lambda^2}{6} \int_{\mathbf{k}, \mathbf{q}} S_0(\mathbf{k}, t) S_0(\mathbf{q}, t) S_0(\mathbf{p} - \mathbf{k} - \mathbf{q}, t), \end{aligned}$$

with

$$\int_{\mathbf{k}} = \int \frac{d^d k}{(2\pi)^d}. \quad (64)$$

After performing all the time integrals and taking the derivatives as in Eq. (60), one may follow the arguments given in [22] for the quantum theory to find the evolution for $\delta T(\mathbf{p}, t) \equiv T(\mathbf{p}, t) - T$ in the relaxation-time approximation. The result is

$$\partial_t \delta T(\mathbf{p}, t) = -\Gamma_{\text{cl}}(\mathbf{p}) \delta T(\mathbf{p}, t), \quad (65)$$

with

$$\Gamma_{\text{cl}}(\mathbf{p}) = -\frac{\text{Im } \Sigma_{R,\text{cl}}(\omega_{\mathbf{p}}, \mathbf{p})}{\omega_{\mathbf{p}}}. \quad (66)$$

On-shell, only the two-to-two scattering contribution in the retarded self-energy is kinematically allowed. This can be written as [25, 26]

$$\begin{aligned} \text{Im } \Sigma_{R,\text{cl}}(\omega_{\mathbf{p}}, \mathbf{p}) = & \\ & -\frac{9\lambda^2}{4} \frac{\omega_{\mathbf{p}}}{T} \int d\Phi_{123}(\mathbf{p}) 2\pi \delta(\omega_{\mathbf{p}} + \omega_{\mathbf{k}} - \omega_{\mathbf{q}} - \omega_{\mathbf{r}}) n_{\text{cl}}(\omega_{\mathbf{k}}) n_{\text{cl}}(\omega_{\mathbf{q}}) n_{\text{cl}}(\omega_{\mathbf{r}}), \end{aligned}$$

where

$$d\Phi_{123}(\mathbf{p}) = \frac{d^d k}{(2\pi)^d 2\omega_{\mathbf{k}}} \frac{d^d q}{(2\pi)^d 2\omega_{\mathbf{q}}} \frac{d^d r}{(2\pi)^d 2\omega_{\mathbf{r}}} (2\pi)^d \delta(\mathbf{p} - \mathbf{k} - \mathbf{q} - \mathbf{r}). \quad (67)$$

Specializing to $d = 1$, we find

$$\Gamma_{\text{cl}}(p) = \frac{9\lambda^2 T^2}{64\pi} I(p), \quad (68)$$

with

$$I(p) = \int_{-\infty}^{\infty} dk \int_{-\infty}^{\infty} dq \frac{\delta(\omega_p + \omega_k - \omega_q - \omega_{p-k-q})}{\omega_k^2 \omega_q^2 \omega_{p-k-q}^2}. \quad (69)$$

Note that the momentum integrals are ultraviolet finite. The integral is invariant under $p \rightarrow -p$, so we may restrict ourselves to $p \geq 0$. The q -integral can be performed using the delta function, which has support at two separated points only, $q = p$ and $q = -k$. The result is

$$\begin{aligned} I(p) &= \frac{2}{\omega_p} \int_{-\infty}^{\infty} dk \frac{1}{\omega_k^3} \frac{1}{|k\omega_p + p\omega_k|} \\ &= -\frac{2}{\omega_p} \int_{-\infty}^{-p} dk \frac{1}{\omega_k^3} \frac{k\omega_p - p\omega_k}{\omega_k^2 - \omega_p^2} + \frac{2}{\omega_p} \int_{-p}^{\infty} dk \frac{1}{\omega_k^3} \frac{k\omega_p - p\omega_k}{\omega_k^2 - \omega_p^2}. \end{aligned} \quad (70)$$

The remaining integrals contain a collinear singularity when $k \rightarrow -p$, leading to a logarithmic divergence. This singularity is present in the quantum self-energy as well. We regulate this in an ad-hoc manner by modifying the integration boundaries to $-p \pm \mu$, with $\mu \ll m$ a small cutoff.

The integrals are straightforward using partial fractioning, and the final result is

$$\Gamma_{\text{cl}}(p) = \frac{9\lambda^2 T^2}{16\pi m^2 \omega_p^3} \left[-1 + \frac{p}{m} \arctan \frac{p}{m} + \ln \frac{2\omega_p}{\mu} \right]. \quad (71)$$

The rate is positive for sufficiently small μ ($\mu/m \lesssim 0.7$). Two limiting cases are

$$\Gamma_{\text{cl}}(0) = \frac{9\lambda^2 T^2}{16\pi m^5} \ln \frac{2m}{\mu}, \quad \Gamma_{\text{cl}}(p \gg m) = \frac{9\lambda^2 T^2}{32\pi m^3 p^2}. \quad (72)$$

Up to now we have silently neglected the corrections to the mass parameter due to interactions. If we denote the resummed mass parameter with M , m has to be replaced by M in the expressions above.

Let us conclude by noting that loosely identifying μ with Γ_{cl} itself gives a relaxation rate $\Gamma_{\text{cl}}(0)$ which is at least two orders of magnitude too big, when compared to the numerical results for the thermalization rate $1/\tau$.

References

- [1] L. Kofman, A. Linde, and A. A. Starobinsky, Phys. Rev. **D56** (1997) 3258 [hep-ph/9704452].
- [2] D. Boyanovsky, H. J. de Vega, and R. Holman, *Erice lectures on inflationary reheating*, in *International School of Astrophysics, D. Chalonge: 5th Course: Current Topics in Astrofundamental Physics*, hep-ph/9701304.
- [3] F. Cooper, S. Habib, Y. Kluger, E. Mottola, J. P. Paz, and P. R. Anderson, Phys. Rev. **D50** (1994) 2848 [hep-ph/9405352].
- [4] F. Cooper, S. Habib, Y. Kluger, and E. Mottola, Phys. Rev. **D55** (1997) 6471 [hep-ph/9610345].
- [5] D. Boyanovsky, D. Cormier, H.J. de Vega, R. Holman, A. Singh, and M. Srednicki, Phys. Rev. **D56** (1997) 1939 [hep-ph/9703327]; D. Boyanovsky, D. Cormier, H.J. de Vega, R. Holman, and S.P. Kumar, *ibid.* **D57** (1998) 2166 [hep-ph/9709232].
- [6] J. Baacke, K. Heitmann, and C. Pätzold, Phys. Rev. **D55** (1997) 2320 [hep-th/9608006]; *ibid.* **D58** (1998) 125013 [hep-ph/9806205].
- [7] C. Destri and E. Manfredini, Phys. Rev. **D62** (2000) 025007 [hep-ph/0001177].
- [8] D. Boyanovsky, M. D'Attanasio, H. J. de Vega, and R. Holman, Phys. Rev. **D54** (1996) 1748 [hep-ph/9602232]; D. Boyanovsky, H. J. de Vega, R. Holman, S. P. Kumar, and R. D. Pisarski, *ibid.* **D58** (1998) 125009 [hep-ph/9802370].

- [9] G. Aarts and J. Smit, Nucl. Phys. **B555** (1999) 355 [hep-ph/9812413]; Phys. Rev. **D61** (2000) 025002 [hep-ph/9906538].
- [10] G. J. Cheetham and E. J. Copeland, Phys. Rev. **D53** (1996) 4125 [gr-qc/9503043].
- [11] B. Mihaila, J. F. Dawson, and F. Cooper, Phys. Rev. **D56** (1997) 5400 [hep-ph/9705354]; B. Mihaila, T. Athan, F. Cooper, J. Dawson, and S. Habib, hep-ph/0003105; B. Mihaila, F. Cooper, and J. F. Dawson, hep-ph/0006254.
- [12] F. L. Braghin, Phys. Rev. **D57** (1998) 6317.
- [13] C. Wetterich, Phys. Rev. Lett. **78** (1997) 3598 [hep-th/9612206].
- [14] L. M. A. Bettencourt and C. Wetterich, Phys. Lett. **B430** (1998) 140 [hep-ph/9712429].
- [15] L. M. A. Bettencourt and C. Wetterich, hep-ph/9805360.
- [16] G. F. Bonini and C. Wetterich, Phys. Rev. **D60** (1999) 105026 [hep-ph/9907533].
- [17] A. V. Ryzhov and L. G. Yaffe, hep-ph/0006333.
- [18] J. Berges and J. Cox, hep-ph/0006160.
- [19] C. Wetterich, Phys. Rev. **E56** (1997) 2687 [hep-th/9703006].
- [20] G. Aarts, G. F. Bonini, and C. Wetterich, Nucl. Phys. **B587** (2000) 403 [hep-ph/0003262].
- [21] H. A. Weldon, Phys. Rev. **D28** (1983) 2007.
- [22] D. Boyanovsky, I. D. Lawrie, and D. S. Lee, Phys. Rev. **D54** (1996) 4013 [hep-ph/9603217].
- [23] G. Aarts and J. Smit, Phys. Lett. **B393** (1997) 395 [hep-ph/9610415].
- [24] W. Buchmüller and A. Jakovác, Phys. Lett. **B407** (1997) 39 [hep-ph/9705452].
- [25] E. Wang and U. Heinz, Phys. Rev. **D53** (1996) 899 [hep-ph/9509333].
- [26] G. Aarts and J. Smit, Nucl. Phys. **B511** (1998) 451 [hep-ph/9707342].